Summer 2022

The Effect of Pulsed Field DC Electrophoresis and Field Amplified Sample Stacking on the Microchip Electrophoretic Separation of Organic Dyes

Travis Geoffrey Stewart

THE EFFECT OF PULSED FIELD DC ELECTROPHORESIS AND FIELD AMPLIFIED SAMPLE STACKING ON THE MICROCHIP ELECTROPHORETIC SEPARATION OF ORGANIC DYES

By

Travis Geoffrey Stewart

Bachelor of Science
University of South Carolina, 2015

Submitted in Partial Fulfillment of the Requirements

For the Degree of Master of Science in

Biomedical Engineering

College of Engineering and Computing

University of South Carolina

2022

Accepted by:

Guiren Wang, Director of Thesis

Yi Wang, Reader

Tracey L. Weldon, Vice Provost and Dean of the Graduate School

Dedication

I dedicate this Master's Thesis to my family. Thank you for your continued love and support.

Acknowledgments

I would like to thank Dr. Guiren Wang, Dr. Yi Wang, Xin Liu, Yukuan Yu, Libo Zhang, Dr. Qian Wang and his lab, and the faculty and staff of the Biomedical Engineering Program for their guidance and support in the completion of this M.S. Thesis and the Biomedical Engineering M.S. Program.

Abstract

The utility of field amplified sample stacking and pulsed field electrophoresis toward improving electrophoretic outcomes was studied with regards to the electrophoretic separation of three organic dyes rhodamine B, 2',7'-dichlorofluorescein, and fluorescein salt in microchip electrophoresis conditions. In this study, there were four experimental groups: nonstacking nonpulsed, nonstacking pulsed, sample stacking nonpulsed, and sample stacking pulsed.

Electrophoretic outcomes were evaluated by examining the electrophoretic separations under an epifluoresence detection method, plotting the signal intensities vs. time, and comparing separation resolutions and signal-to-noise ratios between experimental groups. From this it was shown that sample stacking nonpulsed conditions yielded the best outcome when evaluating the signal intensity vs. time plot. At a distance of 0.750 mm from the microchannel channel cross-section, the separation resolution between RB and DCF was 0.944 in the sample stacking nonpulsed group which was an improvement compared to the separation resolution of 0.885 between dyes RB and DCF in the nonstacking nonpulsed group. However, the separation resolution between DCF and FS in the sample stacking nonpulsed group was worse than that of the same dyes in nonsample stacking nonpulsed group at 0.3933 compared to 0.885. The sample stacking nonpulsed group exhibited the fastest electrophoretic migration of the organic dyes with FS reaching at 0.750 mm in 0.653 seconds and nonsample stacking pulsed was the

slowest group with regards to electrophoretic migration with FS reaching 0.750 mm in 0.959 seconds.

The signal intensities of the fluorescent dyes in the sample stacking groups were significantly lower than those of the nonsample stacking groups and so the potential roles of electrokinetic instability and electrokinetic mixing in preventing signal amplification were investigated. Electrokinetic instability was shown to occur at electric field strengths equal to and greater than 20 kV/m in our MCE setup, suggesting that electrokinetic instability and/or electrokinetic mixing may have been a factor in preventing signal amplification in the FASS groups.

These hindrances to achieving optimal electrophoretic outcomes could be overcome by reducing the switching frequency in pulsed field DC electrophoresis and by reducing the gating and injection voltage in sample stacking conditions. This way, mixing could be reduced in nonsample stacking pulsed and sample stacking pulsed groups and EKI could be reduced in sample stacking and sample stacking pulsed groups and separation outcomes with higher separation resolutions and signal-to-noise ratios could be achieved.

Table of Contents

List of Tables

List of Figures

CHAPTER 1

INTRODUCTION

1.1 Micro Total Analysis Systems

Micro total analysis systems (μTAS) are an important class of microfluidic systems that aim to perform specialized chemical analysis, assays, and other processing steps on a microfluidic chip. μTAS typically use either pressure-driven flows, electrokinetic flows, or a combination of these modalities to manipulate fluids and samples that are being analyzed (Culbertson et al., 2014; Patabidge et al., 2015). The mathematical descriptions of these different fluid flow categories are undergirded by different sets of physical principles. Many existing analytical methods have been minimized into μTAS to reduce the material (e.g. sample volume, buffer volume) and time requirements needed to preform them. The volume required for these μTAS is on the order of picoliters compared to milliliters and the time required for these processes is on the order of seconds as compared to tens of minutes in some cases.

μTAS are useful for analyzing biological samples such as nucleic acids, organelles, proteins, cells, biological tissues, and organ systems. The versatility of μTAS make these systems useful in fundamental biological and physiological research, pharmaceutical research, and medical diagnostic technologies (Colbertson et al., 2014; Patabidge et al., 2015). μTAS can provide various physiological and pathological models for pharmaceutical research to determine the effectiveness and toxicity of drugs while

also reducing the costs by reducing the sample requirements. μTAS that are designed for precise manipulation of mechanical forces in fluids make good systems for miniature models of tissue and organ systems. This manipulation is often carried out by external pressure pumps but can also be driven by capillary forces which can be tailored toward the application with selection of materials and the dimensions of channels or various regions of the chip (usually in analytical systems though instead of modelling systems tmk). μTAS that are designed for electrokinetic manipulation of fluids tend to be focused on separations for identification, quantification, or further processing of samples in a larger microfluidic system. This could be the identification of nucleic acids, proteins, etc the quanitification of nucleic acids, the processing of cells via lysis for electrophoresis and quantification of subcellular components.

1.2 Microchip Electrophoresis

Electrophoresis is one of the analytical methods that has been minimized into a μTAS modality. Electrophoresis is the movement of charged particles in the presence of an electric field. In a biomedical context, these particles could be nucleic acids, cells, amino acids, proteins and any combination of these particles. Particles with different charges move at different speeds in the presence of an electric field. The speeds are directly proportional to the magnitude of the charge and the direction of electrophoresis is determined by the polarities of the charge and the electrodes. Electrophoresis as an analytical method can be used to determine the charge of chemicals in sample from their different velocities in the presence of an electric field but it can also be used to quantify analytes and to identify analytes by comparing results to previously established electrophoretic velocity values of biological analytes.

With the emergence of capillary electrophoresis and later μTAS, electrophoresis was minimized to provide the same results with less sample and less running buffer solution volumes (Bharadwaj et al., 2002; Lacher et al., 2001; Castro & Manz, 2015). This was enabled by the development and application of microfabrication towards μTAS devices requiring the development of new manufacturing process and the utilization of new materials optimized for the context of miniaturized devices. In most applications in which electrophoretic separation is desired, only electrokinetic methods of fluid manipulation are necessary as opposed to pressure-based methods. However, there are studies that combine both modalities by for example designing a microchannel to take advantage of gravity-driven fluid flow (e.g., a ramp/inclination) and combining it with EK separation methods, the induction of a pressure gradient by using materials with different surface properties and combining it with EK separation methods, or the inclusion of an external pressure pump in addition to an external voltage source (Santhiago, 2001).

CHAPTER 2

THEORY

When discussing µTAS, first we need to describe the physics governing the fluids in microfluidic systems. The foundation of the theories that underpin µTAS are grounded in fluid mechanics and electrochemistry. This overview of relevant theory will help elucidate how µTAS can be designed to reach to desired analytical goals. µTAS systems need to be designed to exploit the physics that are prominent at the microscale in comparison to conventional scale systems to achieve the goals of the field - that is fast output with lower sample consumption. This overview includes sets of fundamental equations from the field of fluid mechanics and mass transport adapted to the physical context of microfluidic systems. This equations are fundamental to engineering science and can therefore help to predict the behavior of analytes and systems in µTAS and are useful in the design of µTAS and the experiments that use them. These equations describe the movement of fluids in microchannels, the electrochemical interaction between the materials of the microchannel and the fluid, and the movement of dissolved species in fluid under the influence of an extrinsic electrical field. These equations are important in understanding the EK experiments which are the subject of this Master's thesis and the wider context of microfluidics.

2.1 Navier-Stokes Description of Fluid Flow

The most important equations that describe the nature of fluid flow in microfluidic systems are the Navier-Stokes equations (Viovy, 2000; Santiago, 2001; Zuo

et al., 2014). The Navier-Stokes equations describe the behavior of fluid flow across the total range of possible fluid systems in nature. The first Navier-Stokes equation is a general description of the conservation of mass. The principle of conservation of mass states that the total amount of mass in a closed system remains unchanged over time no matter what forces act upon the system. The second Navier-Stokes equation states the amount of force experienced by a fluid element is equal to the sum of surface forces and body forces experienced by that fluid element. This is a restatement of Newton's second law which states that the force acting on an object is the product of its mass and acceleration.

When expanded to include the influence of an extrinsic electrical field, the N-S equation provides an accurate description of flow generated by an electric force (i.e. electroosmosis). Thus, they are useful in helping in describing and predicting the behavior of fluids in electrophoretic systems.

Navier-Stokes equation with electrostatic source term:

$$\rho \frac{\delta \vec{\boldsymbol{u}}}{\delta t} + \rho \vec{\boldsymbol{u}} \cdot \nabla \vec{\boldsymbol{u}} = -\nabla p + \eta \nabla^2 \vec{\boldsymbol{u}} + \rho_E \vec{\boldsymbol{E}}_{\text{ext}} \quad (1)$$

2.2 Nernst-Planck Description of Mass Transport

While the N-S equation is beneficial in describing the behavior of fluids in microchannels, another equation is needed to describe the movement of dissolved species within these fluids. This is because the goal of μTAS systems isn't just to move fluids, (though such experiments are useful in the study of fluid mechanics), but to analyze various molecular substances. The fundamental equation that describes mass transport in

µTAS systems is the Nernst-Planck equation. The N-P equation describes mass transport by diffusion and convection of dissolved species in microfluidic systems (Lim et al., 2018; Yang & Chien, 2001; Hlushkou et al., 2006). This is relevant because these forces are affecting the species that needs to be analyzed before detection. These equations can help predict the movement of the analyzed species in the µTAS during the MCE process. This provides a good description of movement of charged species due to electrokinetic forces and diffusion which can assist in the prediction of electrophoretic outcomes, such as successful separation and signal-to-noise ratio. Predictably, the goals of the µTAS are to minimize diffusion and to tailor the MCE so that the convective movement of the species reaches the detector with the species at an adequate concentration, i.e. above the detection limit (LOD). The N-P equation can be used to compute the change of concentration over time given the initial concentration of the species, its diffusivity in the solution, and magnitude and direction of the electric field. These are relevant in analysis of biological macromolecules and other chemicals of biomedical relevance because if the charges of the molecules and the concentration of the molecule are known, take for example the charge and concentration of a protein solution, you can determine the speed of its movement through the MCE channel. Conversely, if the identity of the protein is unknown one can use the MCE speed to help determine the identity of the protein. µTAS are designed to take advantage of the forces described in the N-P equation to carry out specific analytical tasks. The dimensions of the channels and the materials of the

chip are selected to optimize the effect of the channels' surface chemistry on species flow.

$$\frac{\partial c_i}{\partial t} = -\nabla \cdot [-D_i \nabla c_i + \vec{\boldsymbol{u}}_i c_i] \quad (2)$$

While pressure-based μTAS are more appropriate for tissue and organ system modeling studies and electrokinetic-based and combination μTAS are more appropriate for separation studies of charged analytes, both categories of μTAS most take account the N-P equation when designing microfluidic chips to optimize μTAS performance. Pressure-based μTAS systems are designed to enable the replication of physiological mechanical forces and mass transport conditions that depend on specialized fluid flows. EK methods can be utilized in μTAS biological models but these high voltage electric fields that are typical of EK μTAS MCE nonphysiological settings that may be counterproductive to the aims of tissue and organ modeling μTAS. EK-based μTAS utilize high voltage power to provide separation and analysis of charged species in rapid time. Pressure-based modalities can be used in EK-based separation-oriented μTAS but the dispersive contribution of pressure-based mass transport (i.e. Taylor dispersion) can ultimately destroy separation resolution if not controlled.

There are two concurrent and overlapping phenomena that influence the nature and the physical development of the electrophoretic process in microfluidic systems. These phenomena are electroosmosis and electrophoresis.

2.3 Electroosmosis (Introduction)

Electroosmosis or electroosmotic flow (EOF) is the movement of water molecules in the presence of an electric field, which is suggested by its etymological roots, “electro” which denotes the electric source of movement and “osmosis” which is defined as the movement of water. This phenomenon arises under special conditions: the presence of an electrical double layer between an electrolyte and a solid surface (i.e. channel wall), a channel small enough that water molecules align across the diameter of the channel when under the presence of an electric field, and a sufficiently strong electric field (Devasenathipathy & Santiago, 2002; Zuo et al., 2014). Without these conditions, the generation of electroosmosis is impossible, therefore the design of MCE systems requires the establishment and maintenance of these conditions.

In addition to electrochemistry and fluid mechanics, surface chemistry is very important in regards to μTAS. Surface chemistry is concerned with the chemical nature of surfaces when in contact with other solids or fluids and the free energy of these surfaces. From the energy of these surfaces, it can be determined whether molecules in a fluid solution will bond with the surface. When an electrolyte is brought in contact with a solid with a charged surface, a spontaneous electrochemical reaction occurs between the liquid and the surface, resulting in a redistribution of charges. EOF will be revisited in greater depth once the theory of the electrical double layer is discussed and its importance in the contribution to EOF is established.

2.4 Electric Double Layer

Electroosmotic flow is enabled by the electric double layer (EDL) that forms between the buffer solution and the channel walls. The buffer solution and the channel material must be selected so that an EDL forms i.e. the pKa needs to be substantially different from the pH of the buffer solution so that the resulting surface charge of the channel walls enables a stable and strong enough EDL to enable the required water molecule alignment via hydrogen bonding across the channel that enables EOF (see Figure 2.1).

In cases where the pKa of the channel wall is lower than the buffer solution pH, the wall will deprotonate. To balance the negative charge of the wall, cations in the buffer solution move towards the wall spontaneiously and forms a double-layered region: one immobile and one mobile. The closest layer to the wall is called the Stern layer and is immobile. The further layer is the Gouy-Chapman layer and is mobile or diffuse (Viovy, 2000; Devasenathipathy & Santhiago, 2002; Messinger & Squires, 2010). The cations in the mobile, diffuse layer move towards the cathode which results in the bulk movement of the fluid towards the cathode in a plug-like fashion due to the hydrogen-bond alignment of the water molecules.

In MCE systems, though the Debye length typically ranges from 0.1-10nm, the influence of the charged surface of the wall extends throughout the width of the channel as a result of the interaction between the cations of the diffuse layer and water moecules

aligned across the microchannel (Hossan et al., 2018). The velocity of the flow can be controlled by adjusting the electric potential at the ends of a microchannel. As long as the electric field is sufficiently strong, a higher electric field strength will cause a higher flow velocity and a lower electric field strength will cause a lower flow velocity.

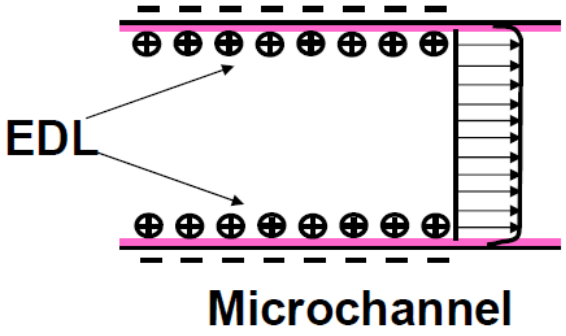

Figure 2.1 Electroosmotic Flow and the Electric Double Layer Schematic by Wang, 2015

2.5 Electroosmosis (Continued)

As has been established, EOF is enabled by the EDL that forms as a result of electrolyte contact with a charged wall and the presence of a strong electric field. For microchannels with negatively charged surfaces like those studied in this thesis, the bulk fluid moves from the cathode to anode in a plug like formation as a result of a high strength electric field. For microchannels with positively charged surfaces, the bulk fluid moves in the opposite direction in response to a high strength electric field. The electric field needs to be strong enough to induce EOF flow, and should also be strong enough to complete the analytical task in adequate time. For most MCE applications,

the electric field strength results in a steady-state EOF flow. While having a prominent EOF is good for certain applications such as electroosmotic pumping and preconcentration of biomolecules, an excessive EOF velocity can cause non-steady state fluid flow and reduce the effectiveness of electrophoretic separations (Messinger & Squires, 2010; Reschke et al., 2010; Santiago, 2003). This is because it produces a counterflow in the direction opposite of electromigration of negatively charged biomolecules such as DNA. Therefore the EOF has to be suppressed in order to optimize electrophoretic outcomes.

Two important electroosmotic flow parameters relevant to experimental measurements follow from this discussion. These parameters will help determine the electroosmotic behavior of a fluid in a microchannel in the presence of an electric field. The first is the electroosmotic mobility, μ_{eo}, of a fluid in a microchannel defined as the ratio of field-specific velocity of the fluid an electroosmotic channel with zero pressure gradient and electric field strength: $\mu_{eo} = u/E$. The electroosmotic mobility is the empirically observed proportionality between electric field and fluid velocity. For cases where Joule heating effects are negligible, the mobility is considered a constant of proportionality for a given wall material and solution chemistry.

2.6 Electrophoresis

Electrophoresis describes the flow of charged particles in solution as a result of an electric potential. "Electro" indicates the electric source of movement as mentioned

earlier while “phoresis” means movement (describing the movement of charged particles in this instance). For a given electric potential, ions move toward or away from an electric potential with a speed that is directly proportional to their charge (Devasenathipathy & Santhiago, 2002; Castro & Manz, 2015; Breadmore, 2012). In MCE systems, this electric potential is provided by an external voltage source. The electrophoretic velocity is a product of the electrophoretic mobility and the electric field. The electrophoretic mobility is a ratio which is directly proportional to the charge of the particle and inversely proportional to both the viscosity of the solution and the radius of the particle. As a result, analytes can be discriminated between based on their charge and particle size. Molecules can be separated based on size by using gels. The velocity of the electrophoretic flow can be controlled in real-time by adjusting the electric potential. Adjusting the electric potential adjusts the EOF velocity along with EP velocity. Additionally, increasing electric potential increases Joule heating which the increases diffusion of the sample solution. These factors must be balanced to achieve desired analytical outcomes.

$$V_{ep} = \mu_{ep} E = (\frac{q}{6\pi\eta r})(\frac{V}{L}) \qquad (3)$$

Here, we see quantitatively that EP velocity is the product of EP mobility and the electric field strength. The electrophoretic velocity and electroosmotic velocity are

components of the convective term in the Nernst-Plank equation. Thus they are critical factors in determining the concentration of analyte over time.

$$\frac{\delta c_i}{\delta t} = -\Delta \cdot [-D_i \Delta c_i + u_i c_i] \quad (4)$$

Solving for concentration as a function of position along the x-axis and time gives the following equation (where the convective velocity equals the net electrokinetic velocity which equals the sum of the electroosmotic and electrophoretic velocities):

$$c(x,t) = \frac{\Gamma}{\sqrt{\pi}\sqrt{4Dt}} \exp\left[-\frac{(x-u_{EK}t)^2}{4Dt}\right] \quad (5)$$

Species with different electrophoretic velocities will separate under an electrophoretic field if given adequate distance and adequate time. Furthermore, depending on the sample, different gels and voltage settings will have to be chosen to fit the analytes being separated.

As long as the analytes have different charge/mass ratios, most analytes can separate in free solution, i.e. in the absence of a separation gel. This includes molecules of biological relevance such as proteins and amino acids in some instances (though in many cases, their separation would be enhanced by the use of a separation gel). Nucleic acids have the same charge/mass ratios across sizes for each major category, so they require separation gels to separate them effectively. Separation gels have internal structures that allow them to discriminate macromolecules by size. These structures result in a larger effective viscosity for the larger molecules and a smaller effective

viscosity for the smaller molecules. Therefore, smaller molecules will migrate faster than the larger molecules.

2.7 Field Amplified Sample Stacking

Field amplified sample stacking is a sample preconcentration method that is useful when the available concentration of a sample is lower than desired (Maia et al., 2011; Hou et al., 2017). Preconentration methods are useful when sample analytes are lower than the limit of detection or the signal-to-noise ratio of the sample is lower than desired. If the concentration of a molecule is lower than the limit of detection, sample preconcentration can bring fluorescent signal above the LOD threshold, which would be useful in determining whether a molecule of interest is in a sample solution. If the signal-to-noise ratio is too low for the analytical goals, sample precocnetration can be used to increase the SNR because accumulation of the sample molecule results in a local amplification of the signal while the area outside of the band remains absent of the sample molecule aside from the normal diffusion.

The sample stacking method that we used for my thesis experiments was the field amplified sample stacking (FASS) method. As the name suggests, FASS is a preconcentration method that utilizes an electric field to achieve the preconcentration of sample ions (Maia et al., 2011; Hou et al., 2017). This preconcentration method requires a conductivity gradient across which the sample ions will locally accumulate

which leads to signal amplification (Santiago, 2003; Yang & Chien, 2001; Ma et al., 2016; Wu et al., 2017, Zhu, 2016) (See Figure 2.2). To produce the required concentration gradient, the buffer solution arrangement for FASS experiments is different from the arrangement for standard gated injection MCE experiments. Whereas the standard gated injection MCE experiment employs only one buffer solution (deionized water in the case of these experiments) throughout the channels, FASS experiments employ two buffer solutions of differing conductivities.

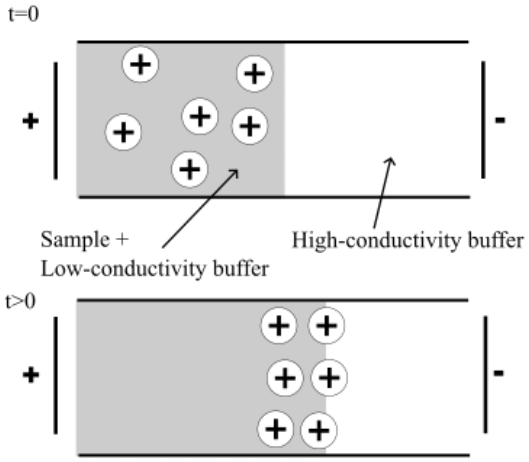

Figure 2.2 The Accumulation of Cations as They Cross the Conductivity Gradient in FASS Conditions

The FASS system can be modeled as a simple circuit where the two buffer solutions represent two resistors in a series circuit powered by the same voltage source. Modeling the FASS scheme as a circuit can help us understand the electric field behaves

in the different buffer regions and how the ions behave across the conductivity gradient. Current remains constant across resistors in a series circuit, and one can use Ohm's law to determine the voltage drop across each resistor in the series. Ohm's law states that voltage drop across a resistor is the product of the electric current flowing through it and the resistance of the resistor. Thus, as a result of this direct proportionality between voltage drop and resistance and the direct proportionality between electric field strength and electrophoretic velocity, the sample moves faster in the low conductivity buffer solution compared to the higher conductivity solution due to the voltage drop being higher across the low conductivity buffer solution compared to the high conductivity buffer solution.

$$V = IR \qquad (6)$$

$$V_{total} = IR_1 + IR_2 \qquad (7)$$

R_1 is resistance of the low-conductivity buffer solution. R_2 is the resistance of the high-conductivity buffer solution. $R_1 > R_2$. Therefore, the voltage drop across R_1 is greater than the voltage drop across the R2. That is, the voltage drop across the low-conductivity buffer solution is greater than the high-conductivity buffer solution. The relationship between voltage and electric field is E = V/L. Both the electroosmotic velocity and the electrophoretic velocity are directly proportional to the electric field

strength. Total electrokinetic velocity is given by the equation $U_{EK} = U_{EP} + U_{EO}$. The electrophoretic velocity of the fluorescent ions and electroosmotic velocity of the buffer solution of the low conductivity region are greater than those of the high conductivity region, which results in stacking of ions at the conductivity interface between regions.

Therefore, when the sample crosses the interface between the two buffer solutions, its velocity will decrease, leading to an accumulation of sample across the interface which will result in signal amplification (Yang & Chien., 2001; Santiago, 2003). This signal amplification can be observed by a fluorescent microscope. The signal amplification can also be captured by a CCD camera and further processed by image processing technology.

2.8 Electrokinetic Instability

While high electric field strengths can be beneficial in enabling electrophoretic separation, they can also lead to electrokinetic instability of fluid flow. This can be manifested as chaotic flow that disturbs the loading step profile or in FASS signal amplification contexts, can result in the breakdown of the conductivity gradient between the two buffer solutions which will destroy signal amplification. (Dubey et al., 2021). This results in mixing at the interface of the high concentration buffer solution and the destruction of the conductivity gradient. As a result, once the conductivity gradient is destroyed, FASS is no longer achievable. Therefore, if the goal is signal amplification,

the process will need to be modified so that the electric field strength is below the threshold for EKI. Electrokinetic instability in FASS contexts is a process that evolves on the order of 3-10 ms, and so experiments that study the evolution of EKI require technology that can record images at the associated framerate (Dubey et al., 2021). Otherwise, it will not be possible to view the evolution of EKI from incidence to full development. The incidence of EKI in the context of FASS conditions occurs as the ions cross the conductivity gradient and is complete once the gradient is destroyed.

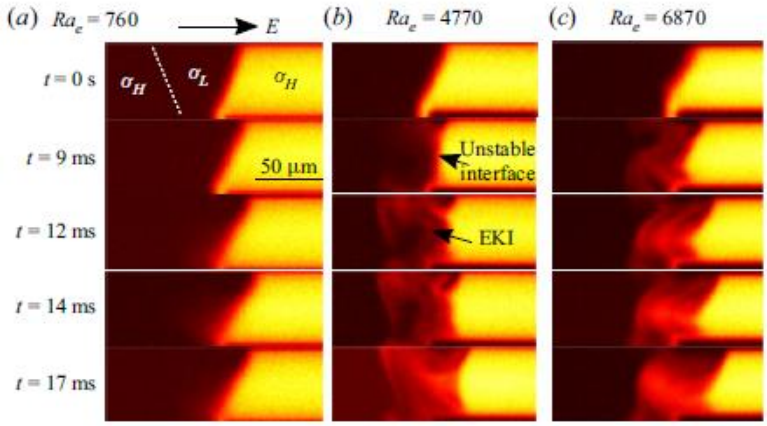

Figure 2.3 Incidence of EKI Across a Conductivity Gradient in MCE Across Rayleigh Values (Dubey et al., 2021)

For our EKI experiments, we studied the interface between 0.5mM HEPES buffer solution and deionized water at electric field strengths in between 10kV/m and 50kV/m to test whether EKI was occurring and to what degree. From the results of these experiments, we determined an optimal range of electric field strengths for FASS

experiments where EKI does not occur. Therefore, we are able to design FASS experiments that maximize signal amplification and signal-to-noise ratio of the fluorescent analytes.

2.9 Fluorescence

Fluorescence is a characteristic of some molecules that causes them to emit light at a specific wavelength as a result of excitation at a lower wavelength light. Fluorescent molecules are excitable at wavelengths of light that are specific to that material and emit wavelengths of light that are also specific to that material. Different fluorescent molecules have different excitation and emission wavelengths, ranging from the visible to the ultraviolet electromagnetic spectrum. Therefore, fluorescent excitation and detection systems must be designed that appropriate for the chemicals that are studied. This is done by the utilization of filters for the mercury lamp and for the detection system. The electrons in the molecule are excited from one orbital to another as a result of the energy the light provides. As the electron returns back to its original orbital state it releases energy in the form of a proton which oscillates at a specific wavelength which is lower than the original exciting proton wavelength.

Some chemicals that are fluorescent in the UV to visible light spectrum are useful in biological and chemical analytical systems. As some biological molecules may not be readily visible in certain contexts, fluorescent tagging can be used to help make them

detectable. These fluorescent materials have proven useful for tagging biological and chemical products to determine whether they are present in certain biological systems and processes and are commonly used in antibody-protein systems to determine whether certain proteins are present in certain biological systems (Wang et al., 2012; Albrecht et al., 2011; Mainz et al., 2012; Mitra et al., 2016; Sahore et al., 2017).

Fluorescence can indicate whether the tagged biomolecule is present and at what quantity. This method can be used in studies of disease progression as well as determining the stage of development in tissue, as different proteins will be present and in different quantities depending on the stage of pathological and/or physiological development. Fluorescent dye also helps us to study velocity profiles and fluid dynamics of electroosmotic processes. Using an electrically neutral dye can help visualize the effect of different electrokinetic modalities on a fluid's velocity profile and the balance of diffusive and convective forces under different electrokinetic and chemical conditions.

CHAPTER 3

MATERIALS

Research in microfluidics requires specialized laboratory equipment and clean facilities to conduct experiments. The material requirements of MCE research include the capacity to generate electroosmotic flow, to adequately visualize fluid flow at the microscale, to maintain the clean conditions needed for microfluidics research, and to induce and detect fluorescence. To achieve the intended goals of our experiment, a specialized laboratory setup was designed to best achieve the desired MCE separation and detection. This laboratory setup included a microfluidic chip, an inverted fluorescent microscope, a mercury lamp, and a high voltage sequencer. The microfluidic chip used for the MCE experiments was the Fluidic 82 cross-channel manufactured by MicrofluidicChipShop GmbH of Jena, Germany. The inverted microscope used to visualize the experiments was the Tokyo Olympus IX70 model. The high voltage sequencer used was the HVS 448 6000D manufactured by LabSmith of Livermore, California. This laboratory setup was used to drive and visualize the separation of fluorescent dyes on a microfluidic chip.

A sample mixture containing the fluorescent dyes Rhodamine B, fluorescein salt, and 2,7-dichlorofluorescein was studied under standard gated injection conditions and under field amplified sample stacking (FASS) conditions. pH7.5 1mM NaCl + 0.5mM

HEPES buffer and pH 7 deionized water were used as the high conductivity and low conductivity buffer solutions, respectively, in FASS experiments. The EC500 ExStik II pH/Conductivity Meter by Extech was used to measure the pH and conductivity values of the buffer solutions used in all of the experiments.

The experiments were recorded using the PCO Sensicam CCD camera manufactured by PCO GmbH and the associated PCO Camware software. PCO Camware and the National Intstitute of Health's ImageJ software were used to process and analyze images from these experiments. Microsoft Excel was used to analyze the processed data from the experiments.

3.1 Organic Dyes

The organic dyes rhodamine B, 2',7'-dichlorofluorescein, and fluorescein salt were used to evaluate the effectiveness of the four MCE experimental groups in achieving electrophoretic separation. These dyes were chosen because of their fluorescence in the visible light spectrum and because of their different formal charges in pH neutral solutions. In pH 7 and pH 7.5 solutions, rhodamine B is a dye with neutral charge, dichlorofluorescein is a dye with -1 charge, and fluorescein salt is a dye with -2 charge (See Tables 3.1 and 3.2).

Table 3.1 List of Fluorescent Dyes Used in MCE with Their Associated Fluorescent Excitation and Emission Wavelengths and Charges in pH 7 and pH 7.5 Solutions.

	Excitation (nm)	**Emission (nm)**	**Charge**
Rhodamine B	546	568	0
2',7'-Dichlorofluorescein	504	529	-1
Fluorescein Salt	475-490	510-520	-2

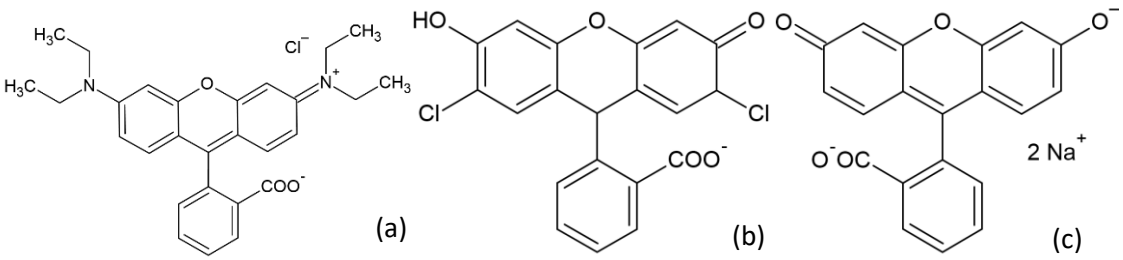

Figure 3.1 Fluorescent Dyes Used in MCE Experiments: (a) Rhodamine B (b) 2',7'-Dichlorofluorescein (c) Fluorescein Salt with Charges Shown as They Would Be in pH 7 and pH 7.5 Solutions.

3.2 Buffer Solutions

Deionized water was used as the separation buffer for the non-FASS MCE experiments. For the FASS experiments, a 0.5mM HEPES + 1mM NaCl solution was used. For the EKI experiments, a 0.5 mM HEPES buffer solution was used.

Table 3.2 Buffer Solutions Used in MCE, FASS, and EKI Experiments and Their pH and Conductivity Values as Measured by the EC500 ExStick pH/Conductivty Meter.

Buffer Solution	**pH**	**Conductivity (µS)**
Deionized water	7	0.0

0.5mM HEPES + 1mM NaCl	7.5	213
0.5mM HEPES + 1mM NaCl	7.5	259

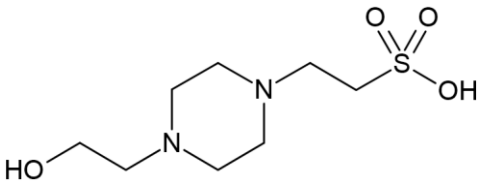

Figure 3.2 HEPES Buffer Chemical Structure

3.3 Microfluidic Chip

The microfluidic chip on which the MCE separation and preconcentration experiments were run was the Fluidic 82 cross-channel microfluidic chip from MicrofluidicChipShop GmbH (Germany). The Fluidic 82 chip is composed of Zeonor, which is a cyclic olefin polymer that is designed to be durable and highly transparent. The horizontal channel is 87.006 mm and the vertical channel is 10 mm. The transparency of the Fluidic 82 microfluidic chip makes it suitable for experiments using visible and ultraviolet light sources for excitation and visualization. The Zeonor microfluidic chip has a pKa of 4.8 which causes the walls to deprotonate in the presence of an electrolyte of pH 7.0 (Mela et al., 2005). This characteristic makes Zeonor a good material for the establishment of an electrical double layer which enables electroosmosis when the channels are filled with water and buffer solutions and subjected to high electric field strength conditions. These characteristics make Zeonor a suitable material for electrophoretic analysis of biologically relevant substances as explained earlier. Zeonor

is compatible with hydrophilic solutions such as alcohols, ketones, etc. but is not compatible and degrades when it comes into contact with hydrophobic solutions.

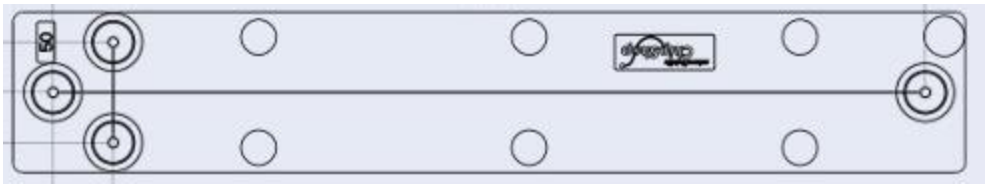

Figure 3.3 Microfluidic ChipShop Fluidic 82 Design, Adapted from Microfluidic ChipShop (2022)

Table 3.3 Microfluidic Chip Material

Material	**pKa**
Zeonor	4.8

3.4 High Voltage Sequencer

Microfluidic electrophoretic experiments require a high voltage source to generate electroosmotic flow. We used the HVS448 6000D high voltage sequencer (LabSmith, California) to power our separation processes. The HVS448 line of high voltage sequencers has been used in many other published μTAS studies to study electrokinetic processes in microfluidics (Mohamadi et al., 2007; Braff et al., 2013; Napoli et al., 2011). The high voltage sequencer and associated software can be used to write and run voltage programs for a maximum of 8 channels which can be can be connected to a microfluidic chip via platinum wires and platinum electrodes as needed. The voltage programs include parameters such as voltage magnitude and time that can be set and sequenced for

each channel. The maximum voltage that can be programmed for each channel is 3000 V. The minimum voltage that can be programmed for each channel is -3000 V.

These programs can be used to apply voltage to the microchip and monitor voltage and current in real-time. However, the rate of output switches is limited by the bus time (the amount of time it takes the computer to send the information to the high voltage sequencer). According to Labsmith, one can switch the voltage of an individual channel at the rate of about 500 Hz (or 2ms) and one can switch the voltage of multiple channels simultaneously at about 100 Hz (or 10 ms) while using the computer interface. The rise-time for voltage-regulated outputs is 0.5 ms, while the speed of current switching is 10-30X slower (LabSmith, 2022). LabSmith also states that running an internal sequence will allow for the HVS to change channel outputs at 0.1 ms (10 kHz) intervals. For our experiments, the voltage sequence is designed only to switch voltage parameters (and does not manually adjust current parameters), and switches multiple channel parameters simultaneously between each step (i.e. loading, gating, and injection steps) though the function (voltage) values of two (of four total) channels do not change between gating and injection steps. (By selecting "unchanged" in the simple sequencer in the HVS software, one can bypass the switch time for a channel if the values are supposed to be equal between steps. In this way, one can optimize the switch times between steps.)

3.5 Inverted Fluorescence Microscope

An inverted optical microscope was used to observe the separation and preconcentration processes on the microfluidic chip. Our inverted fluorescence

microscope uses a mercury arc lamp which produces light that passes through a filter and then is reflected by a dichroic mirror at a 45 degree angle which reroutes the light path to the specimen. The resulting fluorescence is captured by the objective, the light from which passes again through the dichroic mirror. The light reaches a second mirror, from which the light passes through a beam splitter, which splits the light into two paths, one traveling to the eyepiece and the other to the charge coupled device (CCD) camera. A charge-coupled device is an integrated circuit that converts photonic energy to electronic energy.

The CCD camera that we used to monitor and record our experiments was the PCO Sensicam camera along with its associated PCO Camware software. ImageJ was used to analyze the captured recordings.

Chapter 4

Methods

The attraction of micro total analysis systems is their ability to integrate multiple laboratory operations on one chip while using relatively low volumes of sample and buffer solutions when compared to capillary methods and conventional analytical systems. For our microfluidic chip, we are integrating sample stacking, electrophoresis, and fluorescence detection. The loading, injection and separation steps are all electrokinetic processes powered by the HVS 448 6000D high voltage sequencer. The detection is achieved by the inverted fluorescence microscope and the images obtained are recorded and saved using pco Sensicam camera and software.

4.1 Operation of the High Voltage Sequencer and Camera Software for MCE Experiments.

Prior to the operation of the high voltage sequencer for MCE experiments, the PCO Sensicam camera, the mercury lamp, and the microscope and associated tungsten lamp should be powered on. The channels of the chip should be filled with deionized water or with the buffer solution depending on whether you are running a non-FASS or FASS MCE protocol. Then, the sample solution should be placed in the sample reservoir. Place the buffer solution in the sample waste, buffer, and buffer waste

reservoirs. That is, all elements of the chip should be filled with buffer solution with the exception of the sample reservoir.

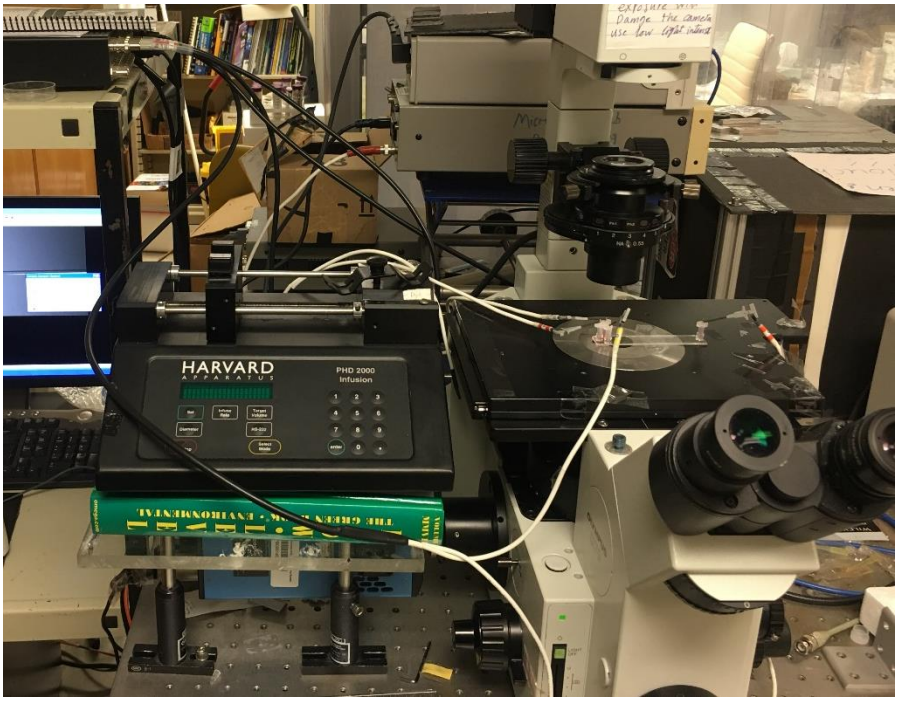

Figure 4.1 MCE Experimental Setup

The cross-channel microchip should be connected to the stage using tape with the cross channel centered above the microscope. The camera exposure settings should be set to a duration that is appropriate for the MCE experiments before selecting the Live Preview function as these settings cannot be adjusted while using Live Preview. Live Preview can be selected to monitor the chip in real-time, which will be necessary to evaluate the MCE experiments and to troubleshoot if necessary. Auto-peak range should

be selected to set the software contrast settings to make everything of interest visible. The contrast settings can be further adjusted using the Contrast B/W button.

If the contrast settings are not adjusted properly, the fluorescent solution in the channel may not be visible. The intensity of the solution in the channel is lower than the sample reservoir, so the contrast may need to be adjusted as one views different areas of the microfluidic chip. Also if the exposure setting is too low in direction the sample solution may not be adequately visible. Once the exposure and contrast settings are adequately set, the Camware software is set for the MCE recording process.

The HVS should be off through these steps until the user is ready to perform the MCE separation experiments. To prepare the chip for the MCE experiments, the user will place the reservoir caps in the reservoirs, insert the electrodes into the reservoirs through the caps, and attach the HVS wires to the electrodes. The wires should be taped down to the stage to prevent the wires from moving during the MCE experiments. This is especially since the wires still exert a moderate amount of tension while the HVS is running and can dislodge electrodes out of the chip in the middle of the experiment, presenting a safety hazard.

After the electrode and wires are connected to the chip, the chip will likely have moved slightly off center above the microscope. The chip should be recentered above the microscope as necessary.

At this point, the high voltage sequencer can be powered on. The high voltage current should be enabled in the HVS software. The sequence wizard in the software should be used to write the voltage program. Once the user is ready to use the voltage

program for the MCE experiments, they must click OK or apply to send the program to the HVS hardware. If the user does not do this, the sequencer firmware will run the last program sent to it as the device has its own internal memory. This presents a potential safety hazard as well. Additionally, having the wrong sequence loaded in the sequencer may cause problems for your experiment. The user will select Run A in the Sequencer or on the HVS Box to Run Step A of the Sequence you sent to the HVS, and so on.

To record the MCE process, the user will need to deselect the Live Preview and then select Record. The monitoring will stop in the interval between when you toggle off live preview and click record. The software will present the last frame previewed as a still image. Once the user selected Record, they will see what the software is recording in real time and the recording can be stopped manually when desired. For simple separation experiments such as the one in this thesis, the user will likely never need more than 200 frames and can probably capture a separation in as little as 60-70 frames, assuming the recording is starting after the loading step has already been established.

Once an image sequence is recorded, it must be saved for later viewing and editing access in Camware and other software. The sequence can be exported in multiple formats including tiff, avi, mpeg formats, but formats outside of tiff have less utility in Camware.

If at any point during your experiment, the user needs to adjust the wires, the high voltage sequence program should be stopped by clicking STOP on the HVS or selecting STOP in the software and then the HVS hardware should be powered OFF. The user should ensure that the wires and/or electrodes are securely attached to the chip before

they turn on the HVS power again. The last sequence sent to the HVS will still be stored in the system even once the system is powered down. Once the user is done with their experiments, or if the user needs to move from the sequencer for any reason the high voltage sequencer should be powered down.

Once the user is done with their experiments and the sequencer is powered down, remove the electrodes and place them back in the electrode container. The wires should be removed from the microscope stage area and placed neatly near the high voltage sequencer. The chip should be cleaned under by flushing with a basic solution such as KOH or NaOH and then flused with deionized water. Camware should then be used to determine whether the chip is clear of fluorescent solution or any fouling that may have occurred during or after the experiemnt. The user should then dry the reservoirs and then place the chip into microchip plastic bag for later use if necessary.

4.2 Gated Injection Method for Microchip Electrophoresis

We chose the gated injection MCE modality because it enables precise control of the length of the sample solution bolus inserted into the designated microchannel for separation (Slentz et al., 2002). The gated injection method consists of three steps: the loading step, the gating step, and the injection step. In our crosschannel scheme, the sample solution reservoir is north, the sample waste solution reservoir is south, the buffer solution reservoir is west and the buffer waste solution reservoir is east. During the loading step, the sample solution travels from the sample reservoir southward to the sample waste reservoir. In the gating step, the leading edge of a sample plug is directed into the separation channel (horizontal channel) from the sample reservoir to the buffer

waste reservoir. For the separation step, the trailing edge of the sample plug is delineated by the buffer solution which helps give it a defined length.

Table 4.1 Voltage Program Parameters for the Gating Injection MCE Method as Programmed in and Executed by the LabSmith HVS488 6000D Sequencer

	Duration (ms)	**A (Sample)**	**B (Buffer Waste)**	**C (Sample Waste)**	**D (Buffer)**	**Next Step**
Loading (V)	(manual switch)	828	1500	0	752	Gating
Gating (V)	300	1000	-3000	300	1000	Injection
Injection (V)	(manual switch)	840	0	840	3000	N/A

4.3 Pulsed Field DC Electrophoresis

Pulsed field DC electrophoresis was investigated as a method to improve separation outcomes. In pulsed field DC electrophoresis, the electrokinetic voltage is programmed to alternate between forward and backwards direction voltage in a square or rectangular wave format. The hypothesis is that with the increased residence time in the separation channel the electrophoretic separation of the dyes would increase and improve separation resolution.

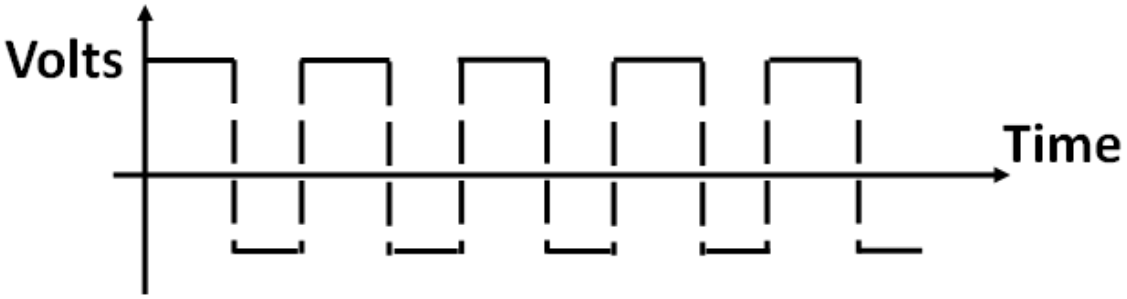

Figure 4.2 General Pulsed Field DC Schematic Which Demonstrates That the Voltage Alternates Between Forward and Backwards Direction in a Rectangular Format. Adapted From Liu, 2019

To program the pulsed field DC electrophoresis method, the original gated injection sequence was modified to add a backward component to the injection step, in which the forward and backwards steps would cycle between each other within a set period. For these experiments, the forward voltage was 3000 V for a period of 100 ms was used and a backward voltage of 2000 V with a period of 50 ms. These settings correspond to a pulse frequency of 6.67 Hz.

Table 4.2 Voltage Program Parameters for the Pulsed DC Gated Injection MCE Method as Programmed in and Executed by the LabSmith HVS488 6000D Sequencer

	Duration (ms)	**A (Sample)**	**B (Buffer Waste)**	**C (Sample Waste)**	**D (Buffer)**	**Next Step**
Loading (V)	(manual switch)	828	1500	0	752	Gating
Gating (V)	300	1000	-3000	300	1000	Injection
Forward (V)	100	840	0	840	3000	Backward
Backward (V)	50	840	2000	840	0	Forward

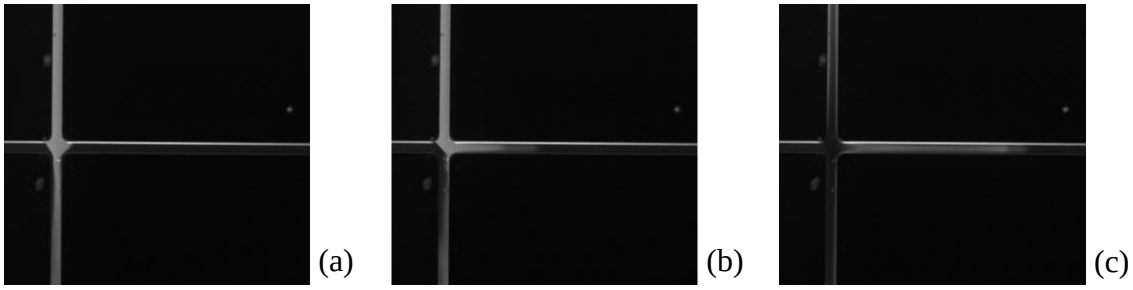
(a) (b) (c)

Figure 4.3 Gated Injection Method Steps for the Nonstacking Nonpulsed Separation of RB, DCF, and FS: (a) Loading Step (b) Gating Step (at 137 ms from Onset of Gating Step) (c) Injection Step (at 274 ms from Onset of Gating step)

4.4 Field Amplified Sample Stacking

As stated before, field amplified sample stacking is a preconcentration method that utilizes a conductivity gradient formed at an interface between two buffer solutions. We use HEPES buffer solution and deionized water to create the conductivity gradient within the separation channel of the microchip. HEPES solution is a pH 7.5 buffer solution that has buffer qualities that are similar to physiological systems.

The gated injection scheme in FASS is modified from the general gated injection scheme as FASS requires introducing two interfacing buffer solutions into the microchannels. In our cross channel scheme, the low conductivity buffer solution is mixed with the sample in the north reservoir, the high conductivity buffer solution is in the sample waste reservoir to the south, the high conductivity buffer solution is in the buffer reservoir to the west, and the high conductivity buffer waste solution reservoir is east. The best way to create the buffer solution arrangement necessary for FASS in our MCE setup is to fill the microchannels with the high conductivity solution from the buffer waste reservoir, dry out the sample reservoir, and then fill the sample reservoir with the sample solution which is mixed with the low conductivity buffer solution.

The conductivity gradient across which the fluorescent sample is stacked is established during the loading step. The sample stacking across the conductivity gradient occurs during the gating and separation steps, two steps that occur in rapid sequence. This causes a local increase in sample concentration and fluorescent signal intensity which was recorded, measured and compared to the MCE trials that did not use sample stacking.

FASS requires two steps to establish the conductivity gradient necessary for the sample preconcentration. The first step includes filling both channels and the sample waste, buffer, and buffer waste reservoirs with the high conductivity buffer solution and then filling the sample reservoir with the sample dissolved in the low conductivity buffer solution. The second step is establishing the conductivity gradient at the crosschannel intersection by using the voltage sequencer to move the sample solution through the sample channel from sample reservoir to sample waste reservoir. During the loading step of the gated injection, the location of the interface between the two solutions will be at the crosschannel on the axis between the buffer and buffer waste reservoirs. These steps enable the chemical conditions that enable the FASS process to take place. The field amplified sample stacking process is initiated by applying an electric field horizontally in the direction of the increasing conductivity gradient.

4.5 Electrokinetic Instability Investigation

Our FASS experimental design was modified to investigate whether EKI occurred at electric field strengths relevant to our FASS experiments. Following the experimental design principles established by Dubey et al, 2021, the rhodamine B dye was dissolved to a concentration of 125 μM in a high conductivity buffer solution (pH 7.5 0.5mM HEPES) while no fluorescent dye was dissolved into the low conductivity buffer solution (pH 7 deionized water). The low conductity buffer solution plug was injected into the separation channel via the pinched injection method and the incidence of EKI was evaluated at electric field strengths of 10-50 kV/m.

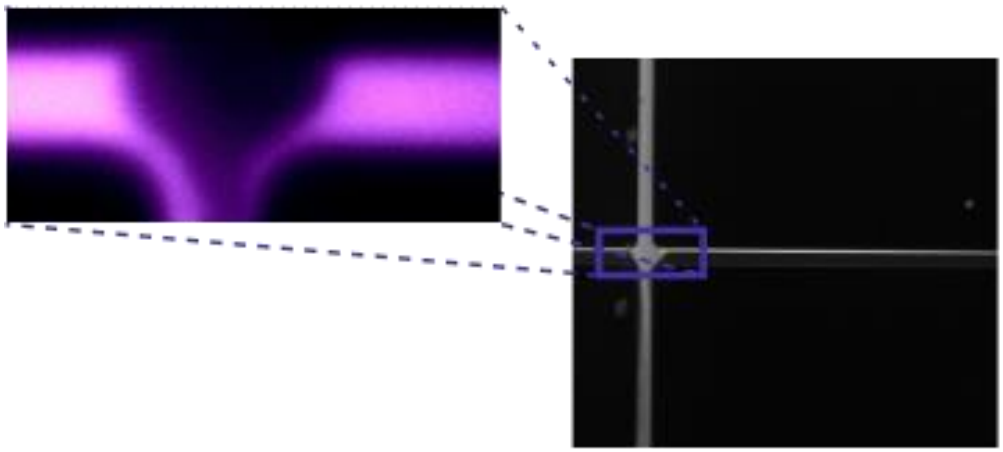

Figure 4.4 EKI location in relation to the cross-channel microchip. EKI occurs at the intersection of the microchip's crosschannel

Table 4.3 Voltage program parameters for the investigation of EKI incidence in FASS MCE conditions as programmed in and executed by the LabSmith HVS488 6000D sequencer

	Duration (ms)	**A (Sample)**	**B (Buffer Waste)**	**C (Sample Waste)**	**D (Buffer)**	**Next Step**
Loading (V)	(manual switch)	828	1500	0	752	Injection
Injection (V)	(manual switch)	840	0	840	870-4350	N/A

4.6 MCE and EKI Visualization using Epifluorescence and Camware

All MCE experiments were visualized using a Tokyo Olympus IX70 inverted fluorescent microscope and a pco.Camware Sensicam CCD camera and associated software. The green filter cube set was used for the MCE non-FASS and FASS experiments while the blue filter cube set was used for the EKI experiments. The exposure setting was 15 ms with 1x1 binning for both non-FASS and FASS experiments leading to framerates of 14.60 Hz and 15.31 Hz, respectively, due to different selected

regions of interest for the camera. The exposure setting for the EKI experiments was 10 ms with 2x2 binning resulting in a framerate of 25.66 Hz.

4.7 Image Processing

We use ImageJ to quantitatively evaluate images to determine fluorescence intensity, signal-to-noise ratio, separation distance, separation resolution, and signal amplification. The resulting data was processed in Microsoft Excel and was analyzed to evaluate the success and effectiveness in the separation and preconcentration of the organic dyes across experimental groups.

4.8 Evaluation of Separation Outcomes

Where peaks could be discerened in the MCE experiments they were shown to follow Guassian distributions. Therefore, the separation resolution equation

$$R = 1.18\,x\,(t_2 - t_1)/(w_{h1} + w_{h2}) \quad (8)$$

was used. In this equation, $t_2 - t_1$ is the time difference between two peaks and w_{hi} is peak width at half height. Additionally, the signal-to-noise ratio was calculated to evaluate the effectivness of the MCE methods in detecting analytes using the equation:

$$SNR = I/(2\sigma) \quad (9)$$

where I is the peak intensity above mean noise level and σ is standard deviation of the background noise (Bharadwaj et al., 2002).

Chapter 5

Results and Discussion

5.1 Microchip Electrophoresis Results

MCE data was analyzed using ImageJ to measure the signal intensity and the distance between the center of the bands. This data was used to calculate and plot the signal-to-noise ratio and resolution for each of the nonstacking and sample stacking conditions. These quantities could be used to determine the effectiveness of each modality towards the desired goals, i.e. improved signal-to-noise ratio and separation resolution. The experimental conditions studied were nonstacking nonpulsed (NSNP) electrophoresis, nonstacking pulsed (NSP) electrophoresis, sample stacking nonpulsed (SSNP) electrophoresis, and sample stacking pulsed (SSP) electrophoresis.

These images were gathered by the PCO Sensicam camera and software under an exposure time of 15ms and a framerate of 14.60 Hz in nonsample stacking conditions and 15.33 Hz in sample stacking conditions. The exposure time was set by the PCO Camware software to cause enough fluorescent excitement (resulting in a higher signal intensity) but also was set low enough to not cause too much background noise. (If the exposure time is too high, the reflected light will be captured by the lens even in areas where there is no sample, resulting in a false positive. This will result in an inaccurate signal-to-noise ratio.) Also, as the exposure time and the framerate are inversely related, the exposure time needs to be low enough to not cause the framerate to be too low.

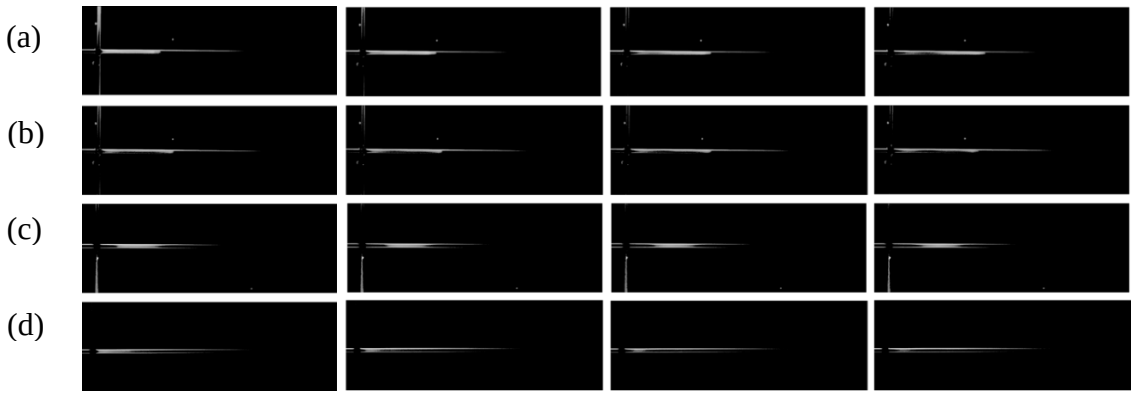

Figure 5.1 Selected Partial Frame-by-Frame Sequences of MCE Experimental Groups. (a) NSNP, (b) NSP, (c) SSNP, (d) SSP. 14.60 Hz Framerate for (a) and (b). 15.31 Hz Framerate for (c) and (d). Time from Onset of Gated Injection: (a) 65.3 ms (b) 130.6 ms (c) 195.9 ms (d) 250.2 ms. Exposure Time: 15 ms.

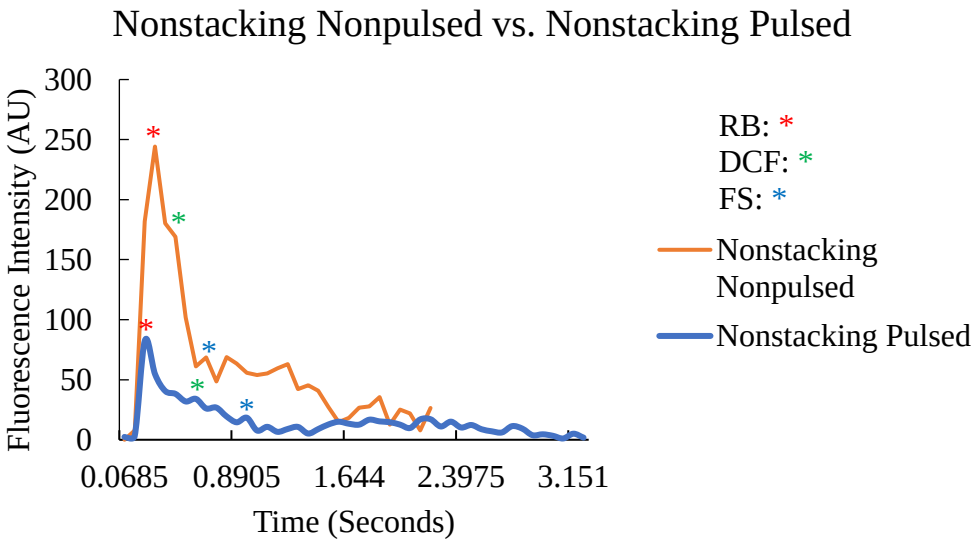

Figure 5.2 Fluorescence Intensity vs. Time MCE Plot, Nonstacking Nonpulsed vs. Nonstacking Pulsed MCE Groups

The separation resolutions, signal-to-noise ratios, and electrophoretic migration times were calculated using ImageJ and Microsoft Excel software for the four MCE experimental groups at a distance of 0.750 mm. The values for each are shown in Tables 4, 5, and 6.

Table 5.1 MCE Separation Resolution for the Four Experimental Groups (NSNP, NSP, SSNP, SSP) Between RB and DCF and Between DCF and FS at 750 µm

	RB and DCF	**DCF and FS**
NSNP	0.885	0.885
NSP	1.9667	1.475
SSNP	0.944	0.3933
SSP	0.59	1.18

The best experimental group for separation resolution of RB and DCF dyes was the NSP group with a value of 1.9667. The worst experimental group for separation resolution of RB and DCF dyes was the SSP group with a value of 0.59. The best experimental group for separation resolution of DCF and FS dyes was the NSP group with a value of 1.475. The worst experimental group for separation resolution of DCF and FS dyes was the SSP group with a value of 1.18.

Table 5.2 MCE Signal-to-Noise Ratios for the Four Experimental Groups (NSNP, NSP, SSNP, SSP) for RB, DCF, and FS at 750 µm

	RB	**DCF**	**FS**
NSNP	6.105	3.939	1.043
NSP	8.031	2.667	0.927
SSNP	2.678	5.77	6.685

SSP	2.194	0.957	0.335

The signal-to-noise ratio for RB is best in the NSP group at 8.031 and worst in SSP group at 2.194. The SNR for DCF is best in the SSNP group at 5.77 and worst in SSP group at 0.957. The SNR for FS is best in the SSNP group at 6.685 and worst in SSP group at 0.335.

Table 5.3 Time in Seconds for RB, DCF, FS to Reach 750 μm in the Four Experimental Groups (NSNP, NSP, SSNP, SSP)

	RB	**DCF**	**FS**
NSNP	0.3425	0.4795	0.685
NSP	0.274	0.6165	0.959
SSNP	0.2612	0.5224	0.653
SSP	0.2612	0.3918	0.653

The NSNP electropherogram shows separation between the 3 dyes but with low separation resolution. In comparison, the NSP electropherogram shows a slight improvement in frame by frame images but a lower signal intensity. This supports the hypothesis set forward by Liu that the higher residence time of pulsed field DC electrophoresis leads to greater separation of the fluorescent dyes within the range of detection when compared to DC electrophoresis.

The SSNP method shows a clear improvement in intensity vs. time plots, but the frame-by-frame screenshots do not show that. As stated before, the MCE separations were analayzed frame by frame at 750 µm using ImageJ to produce the data for the intensity vs. time plots. Though, the MCE separation was not clear visually, analysis using ImageJ showed 3 relatively distinct peaks in the signal intensity vs. time plots of the SSNP method when compared to the NSNP method. However, for the first two resolved molecules, rhodamine B and dichlorofluorescein, the signal intensity of the peaks is lower in the SSNP MCEgram compared to the NSNP group.

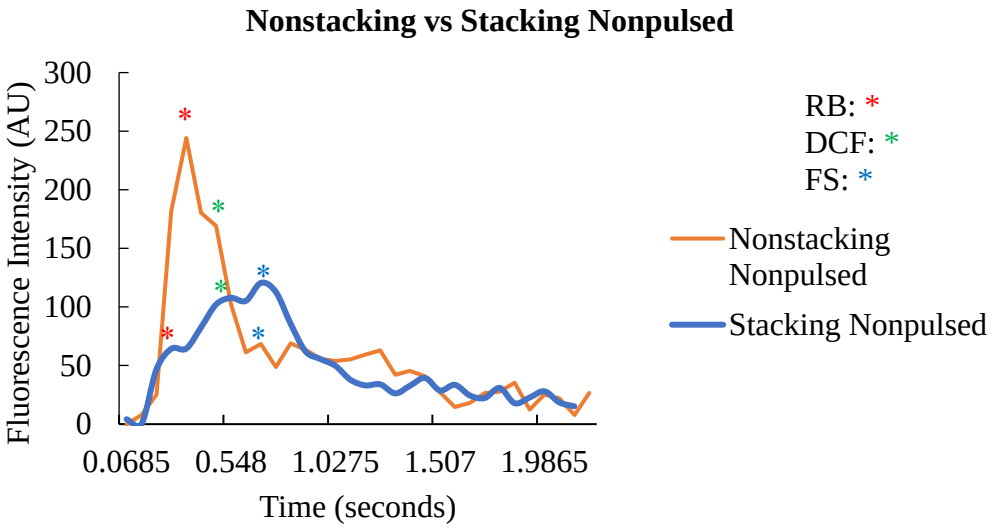

Figure 5.3 Fluorescence Intensity vs. Time MCE Plot, Nonstacking Nonpulsed vs. Stacking Nonpulsed MCE Groups

(a) 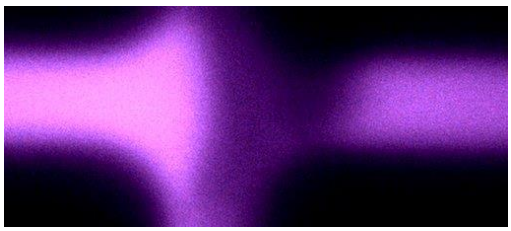 (b) 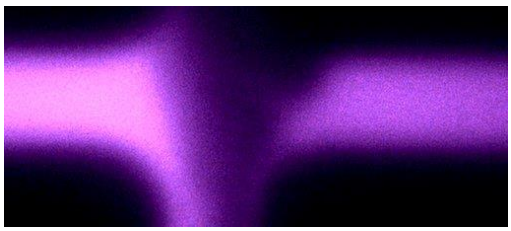

Figure 5.4 Specific Frames in Which EKI is Visible at the Onset of the FASS Process at Electric Field Strengths of (a) 10 kV/m and (b) 20 kV/m. Time after Onset of Pinched Injection (a) 117 ms (b) 156 ms. Note the Ingress of the Fluorescent Sample into the Region That Should be Void of Fluorescent Sample. Exposure Time: 10 ms.

Dubey et al. (2021) have shown that the incidence of EKI contributes to the destruction of the conductivity gradient needed for FASS, so we investigated whether EKI occurred in our FASS settings. EKI was shown to occur in our FASS buffer arrangement at electric fields equal to and greater than 20 kV/m, which suggests that EKI may have been a contributing factor to the lower than expected signal intensity of the SSNP and SSP groups, where the electric field strengths for the gating and injection steps were 46.0 kV/m and 34.5 kV/m, respectively.

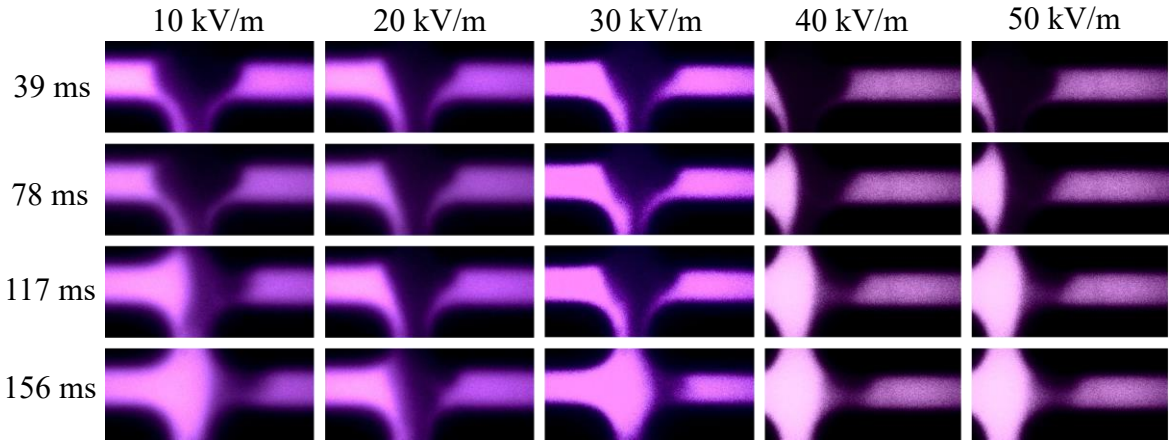

Figure 5.5 Frame-by-Frame EKI Sequence at 10 kV/m. 25.66 Hz Framerate. Exposure Time: 10 ms

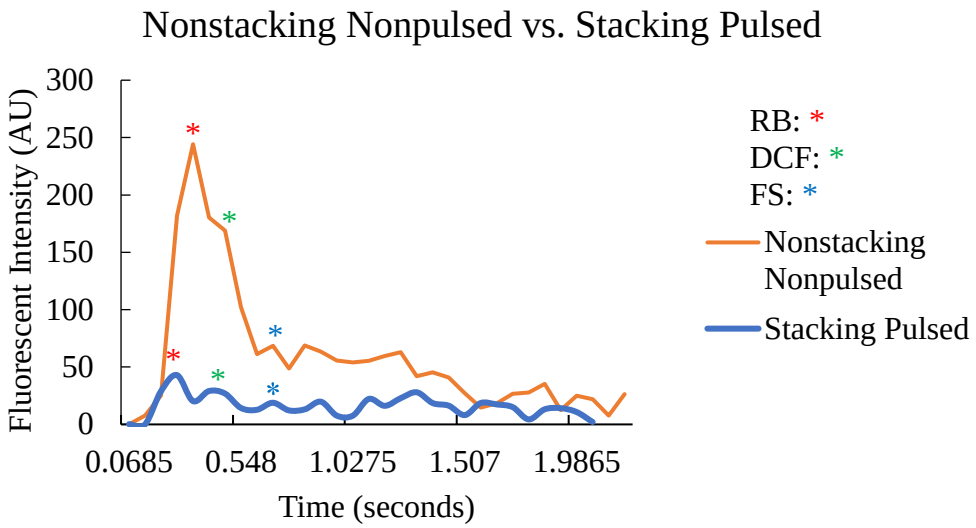

Figure 5.6 Fluorescence Intensity vs. Time MCE Plot, Nonstacking Nonpulsed vs. Stacking Pulsed MCE Groups

The worst experimental group with regards to separation outcomes was the SSP group. It did not show separation of analytes in frame-by-frame images or intensity vs. time plots. Again the incidence of EKI may have contributed to the destruction of the conductivity gradient preventing FASS in our experimental conditions. Additionally, we suggest that the pulsed DC field may be a contributing factor to electrokinetic mixing which is a phenomenon that was highlighted in Zhang et al. (2020) with regards to AC fields in microfluidic conditions. Furthermore, turbulence has been observed to occur at the onset of electric fields in microfluidic conditions by Wang et al. (2014), suggesting that the switching of voltage amplitude and direction that is characteristic of pulsed DC electrophoresis may contribute to mixing and diffusion, leading to poorer electrophoretic outcomes for the NSP and SSP groups.

Chapter 6

Conclusion

In this thesis, we compared four experimental MCE groups. While we saw that sample stacking was better than nonsample stacking in nonpulsed MCE conditions in the signal intensity vs. time plots, the signal intensity was lower than expected given the sample stacking conditions which were expected to lead to signal amplification. We suggest that this signal amplification failure was due to EKI which causes the destruction of conducitivty gradient between buffer solutions, destroying the condition necessary for signal amplification.

In nonsample stacking pulsed DC conditions, judging the frame-by-frame visually, it is apparent that the pulse field DC electrophoresis improves separation outcomes. We argue that this is because of the increased residence time of the sample molecules as a result of this modality. However, judging by the MCE intensity vs. time plots of both the nonsample stacking pulsed and sample stacking nonpulsed groups, the signal intensity is relatively low compared compared to the nonpulsed groups, with low signal-to-noise ratio in both nonsample stacking pulsed and sample stacking nonpulsed groups. We suggest that this may be due to the electrokinetic turbulence and mixing that occurs as a result of the electric force that is cyclically applied to the sample molecules, ultimately causing an increase in diffusion in the MCE process. In sample stacking pulsed conditions, the effects of EKI are compounded by the effects EK turbulence and mixing which results in it having the worst outcomes of the four experimental groups.

We believe that these hindrances to achieving optimal electrophoretic outcomes could be overcome by reducing the switching frequency in pulsed field DC electrophoresis and by reducing the gating and injection voltage in sample stacking conditions. This way, turbulence and mixing can be reduced in nonsample stacking pulsed and sample stacking pulsed groups and EKI can be reduced in sample stacking nonpulsed and sample stacking pulsed groups and separation outcomes with higher separation resolutions and signal-to-noise ratios can be achieved.

References

Albrecht, J. C., Kerby, M. B., Niedringhaus, T. P., Lin, J. S., Wang, X., & Barron, A. E. (2011). Free-solution electrophoretic separations of DNA-drag-tag conjugates on glass microchips with no polymer network and no loss of resolution at increased electric field strength. *Electrophoresis, 32*(10), 1201-1208. doi:10.1002/elps.201000574

Bharadwaj, R., Santiago, J. G., & Mohammadi, B. (2002). Design and optimization of on-chip capillary electrophoresis. *Electrophoresis, 23*(16), 2729-2744. doi:10.1002/1522-2683(200208)23:163.0.co;2-i

Braff, W. A., Willner, D., Hugenholtz, P., Rabaey, K., & Buie, C. R. (2013). Dielectrophoresis-Based Discrimination of Bacteria at the Strain Level Based on Their Surface Properties. *PLoS ONE, 8*(10). doi:10.1371/journal.pone.0076751

Breadmore, M. C. (2012). Capillary and microchip electrophoresis: Challenging the common conceptions. *Journal of Chromatography A, 1221*, 42-55. doi:10.1016/j.chroma.2011.09.062

Castro, E. R., & Manz, A. (2015). Present state of microchip electrophoresis: State of the art and routine applications. *Journal of Chromatography A, 1382*, 66-85. doi:10.1016/j.chroma.2014.11.034

Culbertson, C. T., Mickleburgh, T. G., Stewart-James, S. A., Sellens, K. A., & Pressnall, M. (2014). Micro Total Analysis Systems: Fundamental Advances and Biological Applications. *Analytical Chemistry, 86*(1), 95-118. doi:10.1021/ac403688g

Devasenathipathy, S., & Santiago, J. (2002). Electrokinetic Flow Diagnostics. *Micro- and Nano-Scale Diagnostic Techniques*, 1-45. doi:10.1007/3-540-26449-3_3

Dubey, K., Sanghi, S., Gupta, A., & Bahga, S. S. (2021). Electrokinetic instability due to streamwise conductivity gradients in microchip electrophoresis. Journal of Fluid Mechanics, 925. https://doi.org/10.1017/jfm.2021.672

Fluidic 82 Cross-Shaped Channel Chips [Online image]. (2022). Microfluidic ChipShop. https://www.microfluidic-chipshop.com/catalogue/microfluidic-chips/polymer-chips/cross-shaped-channel-chips/cross-shaped-channel-chips-fluidic-82/

Hlushkou, D., Apanasovich, V., Seidel-Morgenstern, A., & Tallarek, U. (2006). Numerical Simulation Of Electrokinetic Microfluidics In Colloidal Systems. *Chemical Engineering Communications*, *193*(7), 826-839. doi:10.1080/00986440500267295

Hossan, M. R., Dutta, D., Islam, N., & Dutta, P. (2018). Review: Electric field driven pumping in microfluidic device. ELECTROPHORESIS, 39(5-6), 702–731. https://doi.org/10.1002/elps.201700375

HVS448 high voltage power supply for electrophoresis and Microfluidics. LabSmith. (2022, January 21). Retrieved May 11, 2022, from https://labsmith.com/support/hvs448-high-voltage-sequencer/

Jung, B., Bharadwaj, R., & Santiago, J. G. (2003). Thousandfold signal increase using field-amplified sample stacking for on-chip electrophoresis. *Electrophoresis*, *24*(19-20), 3476-3483. doi:10.1002/elps.200305611

Lacher, N. A., Garrison, K. E., Martin, R. S., & Lunte, S. M. (2001). Microchip capillary electrophoresis/ electrochemistry. *Electrophoresis, 22*(12), 2526-2536. doi:10.1002/1522-2683(200107)22:123.0.co;2-k

Lim, A., Lim, C., Lam, Y., & Taboryski, R. (2018). Electroosmotic Flow in Microchannel with Black Silicon Nanostructures. *Micromachines, 9*(5), 229. doi:10.3390/mi9050229

Lin, J., Fu, L., & Yang, R. (2002). Numerical simulation of electrokinetic focusing in microfluidic chips. *Journal of Micromechanics and Microengineering, 12*(6), 955-961. doi:10.1088/0960-1317/12/6/328

Liu, X. (2019). *Experimental Study of Free-Solution Separation Under Pulsed Electrophoresis in Microchip.* (Master's thesis). Retrieved from https://scholarcommons.sc.edu/etd/5318

Ma, B., Song, Y., Niu, J., & Wu, Z. (2016). Highly efficient sample stacking by enhanced field amplification on a simple paper device. *Lab on a Chip, 16*(18), 3460-3465. doi:10.1039/c6lc00633g

Mainz, E. R., Gunasekara, D. B., Caruso, G., Jensen, D. T., Hulvey, M. K., Silva, J. A., . . . Lunte, S. M. (2012). Monitoring intracellular nitric oxide production using microchip electrophoresis and laser-induced fluorescence detection. *Analytical Methods, 4*(2), 414. doi:10.1039/c2ay05542b

Mela, P., Berg, A. V., Fintschenko, Y., Cummings, E. B., Simmons, B. A., & Kirby, B. J. (2005). The zeta potential of cyclo-olefin polymer microchannels and its effects on insulative (electrodeless) dielectrophoresis particle trapping devices. *Electrophoresis, 26*(9), 1792-1799. doi:10.1002/elps.200410153

Messinger, R. J., & Squires, T. M. (2010). Suppression of Electro-Osmotic Flow by Surface Roughness. *Physical Review Letters, 105*(14). doi:10.1103/physrevlett.105.144503

Mitra, I., Snyder, C. M., Zhou, X., Campos, M. I., Alley, W. R., Novotny, M. V., & Jacobson, S. C. (2016). Structural Characterization of Serum N-Glycans by Methylamidation, Fluorescent Labeling, and Analysis by Microchip Electrophoresis. *Analytical Chemistry, 88*(18), 8965-8971. doi:10.1021/acs.analchem.6b00882

Mohamadi, M. R., Mahmoudian, L., Kaji, N., Tokeshi, M., & Baba, Y. (2007). Dynamic coating using methylcellulose and polysorbate 20 for nondenaturing electrophoresis of proteins on plastic microchips. *Electrophoresis, 28*(5), 830-836. doi:10.1002/elps.200600373

Napoli, M., Atzberger, P., & Pennathur, S. (2010). Experimental study of the separation behavior of nanoparticles in micro- and nanochannels. *Microfluidics and Nanofluidics, 10*(1), 69-80. doi:10.1007/s10404-010-0647-7

Nuchtavorn, N., Suntornsuk, W., Lunte, S. M., & Suntornsuk, L. (2015). Recent applications of microchip electrophoresis to biomedical analysis. *Journal of Pharmaceutical and Biomedical Analysis, 113*, 72-96. doi:10.1016/j.jpba.2015.03.002

Oh, K. W. (2012). Lab-on-chip (loc) devices and microfluidics for biomedical applications. MEMS for Biomedical Applications, 150–171. https://doi.org/10.1533/9780857096272.2.150

Patabadige, D. E., Jia, S., Sibbitts, J., Sadeghi, J., Sellens, K., & Culbertson, C. T. (2015). Micro Total Analysis Systems: Fundamental Advances and Applications. *Analytical Chemistry, 88*(1), 320-338. doi:10.1021/acs.analchem.5b04310

Reschke, B. R., Schiffbauer, J., Edwards, B. F., & Timperman, A. T. (2010). Simultaneous separation and detection of cations and anions on a microfluidic device with suppressed electroosmotic flow and a single injection point. *The Analyst, 135*(6), 1351. doi:10.1039/b921914e

Sahore, V., Sonker, M., Nielsen, A. V., Knob, R., Kumar, S., & Woolley, A. T. (2017). Automated microfluidic devices integrating solid-phase extraction, fluorescent labeling, and microchip electrophoresis for preterm birth biomarker analysis. *Analytical and Bioanalytical Chemistry, 410*(3), 933-941. doi:10.1007/s00216-017-0548-7

Santiago, J. G. (2001). Electroosmotic Flows in Microchannels with Finite Inertial and Pressure Forces. *Analytical Chemistry, 73*(10), 2353-2365. doi:10.1021/ac0101398

Slentz, B. E., Penner, N. A., & Regnier, F. (2002). Sampling BIAS at Channel Junctions in Gated Flow Injection on Chips. *Analytical Chemistry, 74*(18), 4835-4840. doi:10.1021/ac020301m

Viovy, J. (2000). Electrophoresis of DNA and other polyelectrolytes: Physical mechanisms. *Reviews of Modern Physics, 72*(3), 813-872. doi:10.1103/revmodphys.72.813

Wang, G.R. (2015). *Micro/Nanofluidics and Lab-on-a-Chip* [PowerPoint slides]. Mechancial Engineering & Biomedical Engineering, University of South Carolina.

Wang, G. R., Yang, F., & Zhao, W. (2014). There can be turbulence in microfluidics at low Reynolds number. Lab Chip, 14(8), 1452–1458. https://doi.org/10.1039/c3lc51403j

Wang, W., Wang, Z., Lin, X., Wang, Z., & Fu, F. (2012). Simultaneous analysis of seven oligopeptides in microbial fuel cell by micro-fluidic chip with reflux injection mode. *Talanta, 100,* 338-343. doi:10.1016/j.talanta.2012.07.079

Wu, Z., Ma, B., Xie, S., Liu, K., & Fang, F. (2017). Simultaneous electrokinetic concentration and separation of proteins on a paper-based analytical device. *RSC Advances, 7*(7), 4011-4016. doi:10.1039/c6ra26500f

Yang, H., & Chien, R. (2001). Sample stacking in laboratory-on-a-chip devices. *Journal of Chromatography A, 924*(1-2), 155-163. doi:10.1016/s0021-9673(01)00856-1

Zhang, L., Beatty, A., Lu, L., Abdalrahman, A., Makris, T. M., Wang, G., & Wang, Q. (2020). Microfluidic-assisted polymer-protein assembly to fabricate homogeneous functionalnanoparticles. Materials Science and Engineering: C, 111, 110768. https://doi.org/10.1016/j.msec.2020.110768

Zhu, F., & Hayes, M. (2016). Exploring gradients in electrophoretic separation and preconcentration on miniaturized devices. Separations, 3(2), 12. https://doi.org/10.3390/separations3020012

Zuo, Y., Wang, G., Yu, Y., Zuo, C., Liu, Z., Hu, D., & Wang, Y. (2014). Suppression of electroosmotic flow by polyampholyte brush. *Microfluidics and Nanofluidics*, *17*(5), 923-931. doi:10.1007/s10404-014-1383-1